

Electron-Doped 1T-MoS₂ via Interface Engineering for Enhanced Electrocatalytic Hydrogen Evolution

Qin Liu,[†] Qi Fang,[†] Wangsheng Chu,[†] Yangyang Wan,[†] Xiuling Li,[†] Weiyu Xu,[†] Muhammad Habib,[†] Shi Tao,[†] Yu Zhou,[†] Daobin Liu,[†] Ting Xiang,[†] Adnan Khalil,[†] Xiaojun Wu,^{†,‡} Manish Chhowalla,[‡] Pulickel M Ajayan,[§] and Li Song^{*,†,‡}

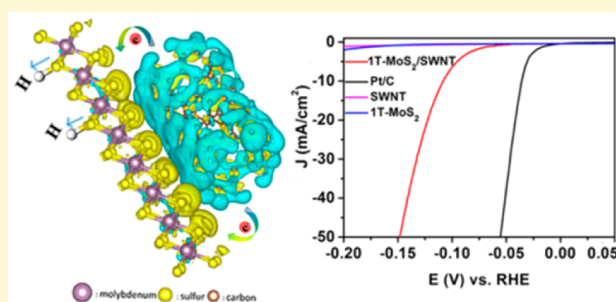
[†]National Synchrotron Radiation Laboratory, CAS Center for Excellence in Nanoscience, Hefei National Laboratory for Physical Science at the Microscale, School of Chemistry, Synergetic Innovation Center of Quantum Information and Quantum Physics, University of Science and Technology of China, Hefei, Anhui 230029, China

[‡]Materials Science and Engineering, Rutgers University, Piscataway, New Jersey 08854, United States

[§]Department of Materials Science and Nano Engineering, Rice University, Houston, Texas 77005, United States

Supporting Information

ABSTRACT: Designing advanced electrocatalysts for hydrogen evolution reaction is of far-reaching significance. Active sites and conductivity play vital roles in such a process. Herein, we demonstrate a heteronanostructure for hydrogen evolution reaction, which consists of metallic 1T-MoS₂ nanopatches grown on the surface of flexible single-walled carbon nanotube (1T-MoS₂/SWNT) films. The simulated deformation charge density of the interface shows that 0.924 electron can be transferred from SWNT to 1T-MoS₂, which weakens the absorption energy of H atom on electron-doped 1T-MoS₂, resulting in superior electrocatalytic performance. The electron doping effect via interface engineering renders this heteronanostructure material outstanding hydrogen evolution reaction (HER) activity with initial overpotential as small as approximately 40 mV, a low Tafel slope of 36 mV/dec, 108 mV for 10 mA/cm², and excellent stability. We propose that such interface engineering could be widely used to develop new catalysts for energy conversion application.



Because of its high energy density and environment-friendly impact, hydrogen is advocated as an alternative energy carrier in the future.^{1,2} Sustainable and efficient production of hydrogen is a prerequisite for realization of the hydrogen economy. Therefore, considerable efforts have been devoted to designing HER electrocatalysts possessing a small overpotential and low Tafel slope.^{3–18} As the most active and chemically stable electrocatalyst for HER, platinum (Pt) suffers from high cost in terms of upscaling; yet it is challenging to find an alternative electrocatalyst to replace Pt. Fortunately, the exploitation of MoS₂ compounds as potential robust and efficient catalysts for HER has opened a promising new path for this field.^{5–8,18,19} Both theoretical and experimental research has proved that increasing the number of metallic Mo edge sites (unsaturated sulfur atoms) is a crucial factor to enhance HER activity.⁶ Great efforts have been made concentrating on improving the number of active edge sites through nanostructuring such as a molecular MoS₂ edge site mimic, amorphous molybdenum sulfides, highly ordered double-gyroid MoS₂ bicontinuous network, MoS₂ films with vertically aligned layers, defect-rich MoS₂ ultrathin nanosheets, MoS₂ nanosheet with strained sulfur vacancies in its basal planes, and so on.^{17–25} Metallic 1T-MoS₂, different from the above semiconducting

2H-MoS₂, possesses Mo–S octahedral coordination, through rotating one of the S–Mo–S basal planes by 60° around the *c*-axis from the trigonal prism 2H structure. Much research has demonstrated that charge transfer kinetics in metallic 1T-MoS₂ is also a key parameter to further improve HER performance.^{26–29} Theoretical calculations show that such 2H-1T phase engineering endows the inert basal plane activation a lowering of ΔG_{H} at +0.18 eV for 1T from +1.6 eV for 2H, equal to 2H-MoS₂ edges on Au(111), known as one of the most active catalysts for hydrogen evolution.³⁰ Similar enhancements in the HER kinetics through intergrading 2H-MoS₂ nanostructures with a variety of conducting supports such as reduced graphene oxide, carbon nanotubes, carbon cloths, and carbon fibers have also been observed.^{31–35} Besides maximizing the active sites at both edge and basal plane, phase engineering, and intergraded 2H phase with conducting substrate, how to further activate and optimize the MoS₂ for hydrogen evolution is still highly desirable. Given the typical ultrathin 2D geometric features of MoS₂, the electronic perturbations derived from the

Received: February 3, 2017

Revised: May 8, 2017

Published: May 8, 2017

support markedly arise, offering an effective means to tailor the catalytic performance.^{36,37} Can electron doping via interface engineering then be used to further optimize the electrocatalytic activity of 1T-MoS₂? The construction of such 1T-MoS₂ heterostructure with an intimate interface still remains a grand challenge due to the traditional lithium intercalation–exfoliation method and stability of the as-obtained 1T phase.^{38–41}

On the basis of our previous works,^{42–44} here we first report metallic 1T-MoS₂ nanopatches with size of ~5 nm in situ bounded to single-walled carbon nanotube films (SWNT) via a bottom-up solvothermal method. 1T-MoS₂/SWNT heterostructure triggered a spontaneous electron transfer between the interface, which weakened the absorption energy of H atom on electron-doped 1T-MoS₂ and thus favors the HER kinetics, dramatically boosting its intrinsic HER activity with a small onset overpotential of ~40 mV, Tafel slope of 36 mV/dec, 108 mV for 10 mA/cm², and high durability. Our unique hybrid nanoarchitecture demonstrates interface engineering-induced electron doping is a promising approach for optimizing the HER kinetics of 1T-MoS₂, and this strategy is expected to benefit the design of cheap and efficient HER electrocatalyst for future clean energy generation.

Figure 1a,b shows a schematic illustration of the synthesis procedure of the 1T-MoS₂/SWNT hybrid samples. Typically,

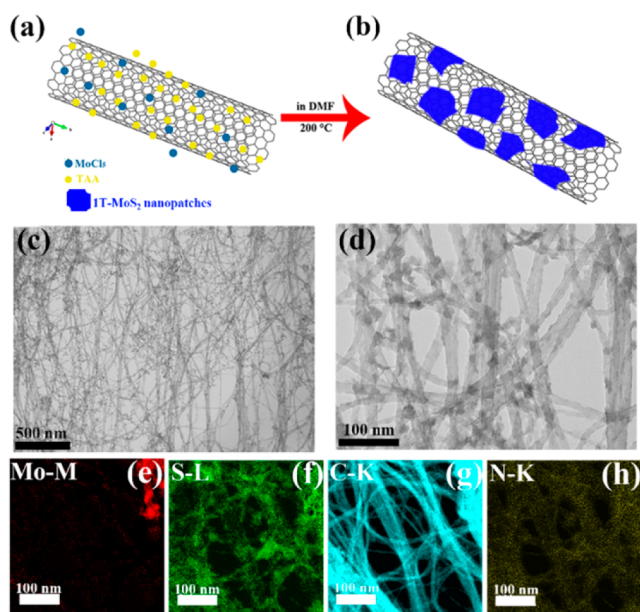


Figure 1. Schematic illustration of the synthesis of 1T-MoS₂/SWNT heterostructure and morphology characterization. (a,b) Schematic illustration of the solvothermal synthesis with SWNT film as substrate for preparation of 1T-MoS₂/SWNT hybrid. (c,d) Low and high magnification TEM images of 1T-MoS₂/SWNT hybrid, which further reveal the hybrid structure where small MoS₂ patches are anchored intimately on the surface of SWNTs. (e–h) EELS elemental mapping of 1T-MoS₂/SWNT heterostructure clearly showing the uniform distribution of molybdenum (red), sulfur (green), carbon (azure), and nitrogen (yellow).

the sample was prepared directly via facial solvothermal method, where MoCl₅ and excessive thioacetamide (TAA) were used as precursors for growing 1T-MoS₂ around the SWNT films (see Figure S1). Notably, a comparison experiment was also conducted under identical synthetic

conditions, resulting in totally different three-dimensional (3D) aggregates of 1T-MoS₂ particles (Figure S2). Thus, we believe that the additional SWNT films can act as a useful support for regulating the growth of loaded materials and fabricating novel functional hybrids. The 1T-MoS₂-coated SWNT hybrids were characterized by means of scanning/transmission electron microscopy (SEM/TEM), as shown in Figure 1c,d (also see Figure S3). The microscopy observations clearly revealed that the compact graphene-like small MoS₂ nanopatches have been in situ grown around the surface of SWNT. Excessive molar ratio of TAA to MoCl₅ plays a vital role for the formation of 1T-MoS₂ structure due to the ammonium ions' intercalation, similar to our previous work (also demonstrated by XRD patterns and Raman spectra in Figure S4).⁴⁴ Furthermore, electron energy loss spectroscopy (EELS) mapping analyses (Figure 1e–h) were utilized to illustrate the elemental distribution. Around the SWNT strand, elements (Mo, S, and N) are also uniformly distributed.

X-ray photoelectron spectroscopy (XPS) was conducted to characterize the chemical state of 1T-MoS₂ on SWNT. The binding energy of Mo 3d in 2H-MoS₂ features two principal peaks at around 229.5 and 232 eV that correspond to Mo⁴⁺ 3d_{5/2} and Mo⁴⁺ 3d_{3/2} components, respectively. Deconvolution of these peaks (Figure 2a) reveals that additional peaks relative

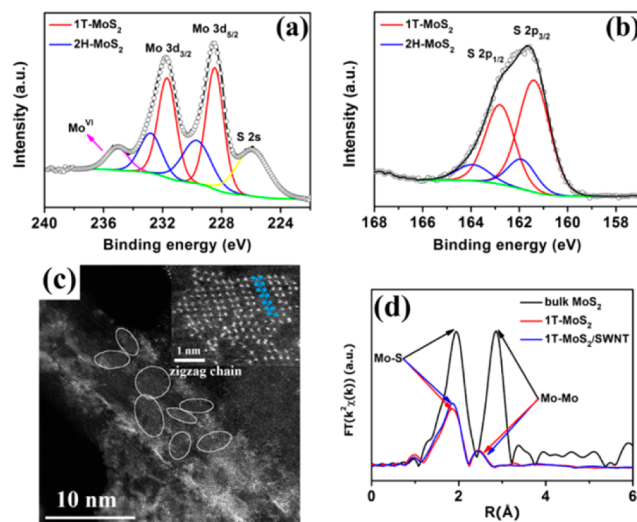


Figure 2. XPS spectra and atomic structural analysis of the 1T-MoS₂/SWNT heterostructure. XPS spectra of Mo 3d (a) and S 2p (b) binding energies of as-prepared 1T-MoS₂/SWNT. The curves are deconvoluted by Gaussian fitting. (c) Typical HADDF-STEM images of 1T-MoS₂/SWNT, showing MoS₂ nanopatches coated SWNT and the obvious zigzag chain pattern of the Mo atoms. The inset magnified image displays a Mo–Mo bond length of 2.75 Å, characteristic of the distorted 1T structure. (d) Fourier transforms of the κ^2 -weighted EXAFS oscillations of the as-prepared samples.

to the position of the 2H-MoS₂ peaks are shifted to lower binding energies. Besides, small peaks for the +6 valence state arise. Similarly, down-shift of bonding energies also appears in the S 2p_{1/2} and S 2p_{3/2} peaks as compared to doublet peaks of 2H-MoS₂ (Figure 2b). The downshift in the peak position of Mo 3d and S 2p peaks indicates that they originate from the 1T phase, which is similar to our previous reports of ammonium ion-intercalated MoS₂.⁴³ The high-resolution XPS spectra of C 1s binding energy (Figure S5a) can be deconvoluted into two peaks. The main peak at 284.6 eV belongs to sp² graphite-like

carbon atoms, and the peak around 286.0 eV is assigned to the carbon atom bound to the oxygen-containing group due to acid treatment. Because of the oxygen group, SWNT possesses not only a more favorable interaction with MoCl₅ and TAA molecules but also better wettability. The existence of intercalated-ammonium ions is also demonstrated by N 1s peak (Figure S5b), similar to our previous report.⁴³ The compositional analysis of XPS (Table S1) shows that the mass fraction of 1T-MoS₂ for the 1T-MoS₂/SWNT sample is around 60%.

The distribution and the atomic arrangement of 1T-MoS₂ nanopatches grown on SWNT were observed directly by the high angle annular dark field image in a spherical aberration-corrected scanning transmission electron microscope (HAADF-STEM). Figure 2c shows that most of the MoS₂ nanopatches tightly lay flat around the nanotube's surface, and some of them possess folded edges corresponding to the different layers of MoS₂ (number of layers = 1–3; see Figure S6). The inset image in Figure 2c shows the high-resolution STEM of grown MoS₂ nanopatches, which reveals that these small MoS₂ patches are just about 5 nm with highly exposed edges. Besides, MoS₂ nanopatches exhibit zigzag chain patterns with a Mo–Mo bond length of 2.75 Å, the characteristic of the distorted 1T phase. X-ray absorption fine spectroscopy (XAFS) at the Mo K-edge, including the extended X-ray absorption fine structure (EXAFS) and X-ray absorption near-edge spectroscopy (XANES), was used to probe the partial electronic and the local geometric structures of the prepared samples, to further confirm zigzag chain superlattice in 1T-MoS₂/SWNT and the interaction between 1T-MoS₂ and SWNT in the electronic/atomic level. Figure 2d shows that the substantial changes in the local atomic structure can be confirmed by the Fourier transform (FT) profiles in the real space (R-space). The FT curves of 2H-MoS₂ as two main peaks at 2.41 and 3.18 Å correspond to the nearest Mo–S and Mo–Mo bonds, respectively. By contrast, the FT curves of 1T-MoS₂ and 1T-MoS₂/SWNT show that the Mo–Mo peak shifts to lower value as compared to 2H-MoS₂, a significant downshift from 3.18 to 2.75 Å. It means that a much shorter bond length of Mo–Mo exists in the 1T-MoS₂/SWNT sample, agreeing with the STEM result. Moreover, both peak intensities of the Mo–Mo and Mo–S bonds are reduced remarkably. Such reduced Mo–Mo bond length and coordination number of the Mo–Mo bond are the typical characteristics of the 1T phase. Moreover, the ultrasmall size of 1T-MoS₂ further reduces the coordination number. The nearest Mo–S bond length slightly becomes shorter probably due to the defects caused by solvothermal treatment or interface effect in the presence of the heterojunction structure. These corresponding FT curves are fitted via the ARTEMIS model to obtain the quantitative parameters of the local structure near the element Mo.⁴⁵ The fitting results are summed in the supplement (Table S2 and Figure S7).

Although a similar geometrical structure was revealed by the EXAFS technique, the XANES spectrum of 1T-MoS₂/SWNT at Mo K-edge shows an obvious energy shift at the rising edge with respect to that of pure 1T-MoS₂, as shown in Figure 3a. This XANES edge downshift is a typical indication that electron transfer occurs from the SWNT to the 1T-MoS₂ nanopatches. Moreover, the position of the XPS C 1s line of 1T-MoS₂/SWNT is also upshifted by ~0.35 eV as compared to the pristine SWNT sample (Figure 3b). We propose that both shifts in the 1T-MoS₂/SWNT hybrid can be related to electron

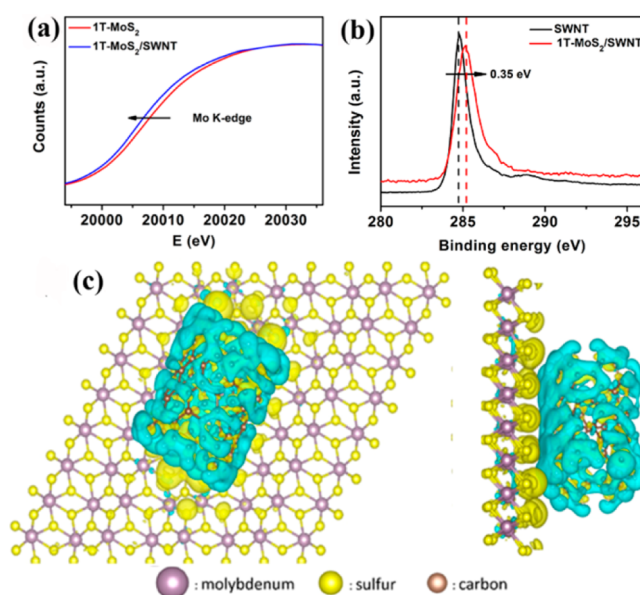


Figure 3. Theoretical simulation and calculation of electron transferring cross the interface. (a) XANES spectra at Mo K-edge of 1T-MoS₂ and 1T-MoS₂/SWNT. (b) XPS C 1s spectra of 1T-MoS₂ and 1T-MoS₂/SWNT. (c) Top (left) and side (right) views of the deformation charge density of interface between 1T-MoS₂ fragment and SWNT, with an isovalue of 0.0002 e/bohr³. Yellow shape represents that the area obtains electrons, while the blue shape represents that the area loses electrons, respectively.

transfer from the SWNT core to the 1T-MoS₂ sheath.⁴⁶ To verify the proposed charge transfer between 1T-MoS₂ fragment and SWNT, we carried out the simulation of deformation charge density. The interface of hydrogen-terminated 1T-MoS₂ with 8 × 4 × 1 lattice and metallic (4, 4) SWNT with 1 × 1 × 4 lattice was considered by first-principle calculation. The simulated deformation charge density of the interface is shown in Figure 3c. It is noticeable that 1T-MoS₂ can attain an electron from SWNT, and the electron transfer mainly occurs on the upper surface of 1T-MoS₂ and on the whole nanotube surface. The further Bader charge analysis indicates that 0.924 electron can be transferred to the 1T-MoS₂ fragment from SWNT, which explains the above downshift in XANES of Mo edge for 1T-MoS₂/SWNT hybrids in contrast with the pure 1T-MoS₂ sample. Thus, we can conclude that such few-nanoscale metallic 1T-MoS₂ nanopatches were in situ grown on a highly conducting SWNT surface, subsequently resulting in electron doping in 1T-MoS₂ nanopatches from SWNT support via an intimate interface. Considering the electron transfer from SWNT to 1T-MoS₂ due to such strong electronic coupling at the tight interface, we further provided first-principles calculations based on density functional theory (DFT) to probe into the adsorption behavior of hydrogen atom on negatively charged 1T-MoS₂ with zigzag edge (see Figure S8 and Table S3). According to previous theoretical calculations,⁴⁷ two kinds of S atoms were studied in our case. Comparing the adsorption energies, the H adsorption energy of negatively charged zigzag-MoS₂ reduces in contrast with that of pure 1T-MoS₂. The calculated adsorption energy and the S–H bond length are summarized in Table S3. Our theoretical calculations well authenticate that for electron-doped 1T-MoS₂, the adsorption capacity of H atom on its surface is weakened, indicating that the following H recombination and release

process in the 1T-MoS₂/SWNT heteronanostructure becomes relatively easier than the pristine ones.

To demonstrate the advance of designed 1T-MoS₂/SWNT hybrids, we studied the electrocatalytic properties of the samples. The HER measurements were performed via a three-electrode setup in 0.5 M H₂SO₄ solution. All polarization (*C*–*V*) curves are not rectified for *iR* loss here. The polarization curves of different catalyst loading amounts and 1T-MoS₂/SWNT ratios were conducted in Figures S9 and S10. Figure 4a

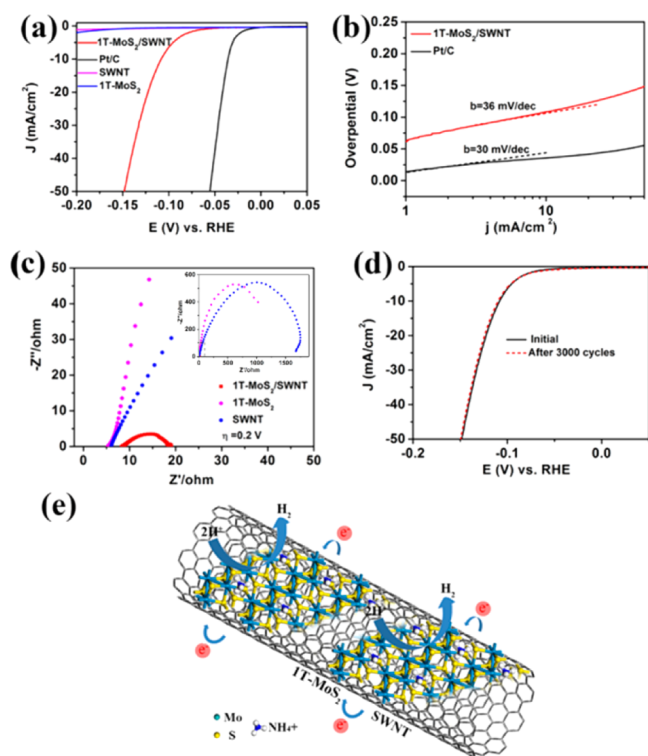


Figure 4. Electrocatalytic hydrogen evolution of different catalysts. (a) Polarization curves of 1T-MoS₂/SWNT heteronanostructure, pure 1T-MoS₂, pure SWNT, and a high-quality commercial Pt catalyst and (b) Tafel plots of 1T-MoS₂/SWNT hybrid and Pt catalyst. Sweep rate: 10 mV s⁻¹. (c) Electrochemical impedance spectra of 1T-MoS₂/SWNT hybrid, 1T-MoS₂, and SWNT at –0.20 V vs RHE from 100 kHz to 0.01 Hz. The inset image shows zoom-out spectra. (d) Durability test for the 1T-MoS₂/SWNT electrocatalyst. (e) HER scheme for 1T-MoS₂/SWNT hybrid catalyst.

shows the polarization curve with 1T-MoS₂/SWNT hybrid electrode. It demonstrates that the 1T-MoS₂/SWNT electrocatalyst possesses a low onset overpotential (η) of ~ 40 mV versus RHE (Figure S11), above which the HER current density increases rapidly. The HER performances of commercial Pt (20 wt % Pt/C) catalyst, 1T-MoS₂, and SWNT were also conducted in the same experimental setup. The Pt/C catalyst exhibits negligible onset overpotential, which is the best electrocatalyst. Bare 1T-MoS₂ presents low HER activity because of the relatively low conductivity and limited exposed active sites of 3D aggregates of 1T-MoS₂ particles. The potential value at 10 mA/cm² is frequently used as a typical reference metric to evaluate the electrochemical catalytic property.¹⁷ Our 1T-MoS₂/SWNT electrocatalyst just needs 108 mV to reach 10 mA/cm².

To understand the underlying mechanism of 1T-MoS₂/SWNT HER catalytic activity, Tafel plots produce a slope of

approximate 36 mV/decade (Figure 4b), which is nearing the value of commercial Pt catalyst with approximately 30 mV/decade. This indicates a possible Volmer–Heyrovsky reaction path, which means that electrochemical hydrogen desorption is the rate-limiting step.²⁵ According to the above characterizations, we suggest that the exceptionally low Tafel slope of 1T-MoS₂/SWNT catalyst corresponding to the substantially improved reaction kinetics can be attributed to the strong chemical and electronic coupling at the interface, which was demonstrated by the above theoretical calculations. It indicates that the reduced H atom absorption energy in such a heteronanostructure makes hydrogen desorption much easier. Chemical coupling/interactions afforded a highly dispersed growth of 1T-MoS₂ nanopatches around SWNT surface without aggregation. The high dispersion and small size of 1T-MoS₂ around SWNT in turn endowed lots of accessible active catalytic sites. Besides, the strong electrical coupling to the SWNT in an interconnected conductive network provided fast electron transfer from the electrodes to the metallic 1T-MoS₂ nanopatches. The rapid charge transfer from the abundant active sites to the glassy-carbon electrodes could also be characterized by electrochemical impedance spectroscopy, which is carried out at $\eta = 0.20$ V vs RHE to study the electrode kinetics under HER process, as shown in Figure 4c. The 1T-MoS₂/SWNT electrocatalyst exhibits substantially lower charge transfer resistance (R_{ct}) than that of bare SWNT and 1T-MoS₂, as shown in Figures S12 and S13. The significantly reduced R_{ct} afforded markedly faster HER kinetics with the 1T-MoS₂/SWNT hybrid catalyst. The intrinsic per-site activity is a vital indicator for evaluating the electrocatalyst. The electrochemical capacitance surface area measurements were used to evaluate the active surface area of the electrocatalyst (see Figure S14).⁴⁸ The double-layer capacitance (C_{dl}) of our as-obtained 1T-MoS₂/SWNT sample is 230.9 mF/cm², which is nearly 45 times higher than the reported value of similar molybdenum sulfide/N-doped CNT forest hybrid catalysts.³² The BET specific surface areas of 1T-MoS₂/SWNT nanocomposites and bare MoS₂ were conducted in Figure S15. The BET specific surface areas of 1T-MoS₂/SWNT nanocomposites and bare MoS₂ were 603.327 and 1.349 m²/g, respectively. The value of 1T-MoS₂/SWNT is 447 times that of 1T-MoS₂, which is well consistent with the above C_{dl} value.

Meanwhile, catalytic durability is another important parameter for the HER catalyst. The catalytic stability of our 1T-MoS₂/SWNT catalyst was measured by continuous cyclic voltammetry conducted from –0.20 to 0.10 V vs RHE with 50 mV/s sweep rate (Figure 4d). The chronoamperometry (*j*–*t*) curve (see Figure S16) demonstrated the long-term stability of 1T-MoS₂/SWNT composite. Even after a long period of 30 000 s, the degradation of current density can be ignored. Negligible deterioration of cathodic current is observed after 3000 cycles, indicating the excellent stability of the material. The good chemical stability of 1T-MoS₂/SWNT catalyst is also demonstrated (see Figure S17), indicating that the HER activity slightly deteriorates even after 6 months of storage in air atmosphere. The TEM image (see Figure S18a) of the sample after the durability test shows that the morphology of 1T-MoS₂ nanopatches coated around SWNT presents negligible alterations after a long period of cycles. The XPS spectra (see Figure S18b,c) of the sample also present no significant alteration in the valence state of Mo and S after the 30 000 s electrochemical process, which confirms the superior stability of the 1T-MoS₂/SWNT sample for long periods of

electrochemical cycling. All of the above results prove that 1T-MoS₂/SWNT catalyst has superior HER activity and stability that is expected to be a very promising electrocatalyst for practical clean hydrogen production (see Table S4).

For better understanding, Figure 4e shows the HER scheme for 1T-MoS₂/SWNT heteronanostructure catalyst according to the above analysis. The remarkable HER activity as well as the high durability of the 1T-MoS₂/SWNT catalyst with multiple synergistic structure and electronic regulations can be ascribed to the following four aspects: (i) the weakened H atom bond energy in electron-doped 1T-MoS₂ via interface engineering makes the H recombination and release easier in the electrochemical hydrogen evolution process; (ii) the metallic characteristic of electron-doped 1T-MoS₂ and SWNT affords a rapid electron transport channel between the electrodes and positive protons, facilitating HER kinetics process; (iii) the just about 5 nm size of ultrasmall 1T-MoS₂ nanopatches in which edges and basal surface are catalytically active offers a proliferated density of catalytic active sites; and (iv) 1T-MoS₂ highly stabilized by interlayered NH₄⁺ and strongly interacted with SWNT ensures its stability against long-term electrocatalysis and aging. In general, collaborative optimization of 1T-MoS₂/SWNT heteronanostructure electrocatalyst by nanostructuring, phase engineering, and interface engineering was realized for one of the most excellent MoS₂-based electrocatalytic hydrogen evolution. Such electron doping via interface engineering may pave a new path to improve the performance of various catalysts.

In conclusion, electron doping of 1T-MoS₂ by in situ forming heteronanostructure has been shown to be an efficient new route for improving its electrocatalytic activity. The induced interfacial electron transfer in such system weakens the absorption capacity of H atom on electron-doped 1T-MoS₂, thus promoting the HER kinetics. The heteronanostructure was shown to be an excellent electrocatalyst for hydrogen evolution reaction and displayed a small onset overpotential, low Tafel slope, and high durability. The methodology of electron doping via interface engineering could also be a general way of improving conductivity in two-dimensional materials (transition metal dichalcogenides and oxides). Our work thus can be extended to more materials beyond MoS₂ and may have wide implications for reactions beyond HER.

■ ASSOCIATED CONTENT

● Supporting Information

The Supporting Information is available free of charge on the ACS Publications website at DOI: 10.1021/acs.chemmater.7b00446.

Pure SWNT characterization, TEM of pure 1T-MoS₂, morphology characterization of 1T-MoS₂/SWNT hybrid, XRD patterns and Raman spectra of pure 1T-MoS₂, XPS spectra of 1T-MoS₂/SWNT heteronanostructure, HAADF-STEM images of 1T-MoS₂/SWNT heteronanostructure, EXAFS analysis, first-principle calculations on the adsorption behavior of hydrogen atom on negatively charged zigzag-MoS₂, polarization curves at various 1T-MoS₂/SWNT loading weight of catalyst, polarization curves at different ratios of 1T-MoS₂ and SWNT, onset overpotential, corresponding fitted electrochemical impedance spectra, electrochemical impedance spectra, capacitance measurements, BET specific surface area, time dependence of current density (*j*-*t* curve) at

static overpotential of 150 mV vs RHE, stability of 1T-MoS₂/SWNT heteronanostructure under air atmosphere, TEM and XPS of the 1T-MoS₂/SWNT sample after stability test, atomic content of Mo, S, C, and N elements obtained from XPS data of 1T-MoS₂/SWNT sample, local structural parameters for adsorbed Mo in bulk 2H-MoS₂, 1T-MoS₂, and 1T-MoS₂/SWNT fitted from EXAFS data, calculated adsorption energy and S-H bond length, and comparison of electrocatalytic HER activity in acidic conditions for 1T-MoS₂/SWNT heteronanostructure with previously reported MoS₂-based HER catalysts (PDF)

■ AUTHOR INFORMATION

Corresponding Author

*E-mail: song2012@ustc.edu.cn.

ORCID

Xiaojun Wu: 0000-0003-3606-1211

Li Song: 0000-0003-0585-8519

Author Contributions

Q.L. and Q.F. contributed equally to this work. L.S. supervised the project. Q.L. and Q.F. carried out most of the experiments and analyzed the data. Y.W., X.L., and X.W. carried out the theoretical modeling and calculations. W.X. and M.H. provided the SWNT film. W.C. and S.T. conducted the EXAFS analyses. Y.Z., D.L., T.X., and A.K. analyzed the electrochemical data. L.S., Q.L., X.L., Y.W., W.C., X.W., and P.M.A. cowrote the paper. M.C. gave advice for this paper. All authors discussed the results.

Notes

The authors declare no competing financial interest.

■ ACKNOWLEDGMENTS

We acknowledge the financial support of the 973 (2014CB848900) Program, the NSFC (11375198, U1532112, 11574280, 11605201), Strategic Priority Research Program of CAS (XDB01020300), China Postdoctoral Science Foundation (2017M612105), and National Postdoctoral Program for Innovative Talents (BX201600141). L.S. thanks the recruitment program of global experts, the CAS Hundred Talent Program. We thank the Beijing Synchrotron Radiation Facility (1W1B and soft-X-ray Endstation, BSRF), the Shanghai Synchrotron Radiation Facility (14W1, SSRF), and the Supercomputer Centers (USTCSCC, SCCAS, Tianjin and Shanghai) for help in characterizations.

■ REFERENCES

- (1) Dresselhaus, M. S.; Thomas, I. L. Alternative Energy Technologies. *Nature* **2001**, *414*, 332–337.
- (2) Turner, J. A. Sustainable Hydrogen Production. *Science* **2004**, *305*, 972–974.
- (3) Greeley, J.; Jaramillo, T. F.; Bonde, J.; Chorkendorff, I.; Nørskov, J. K. Computational High-Throughput Screening of Electrocatalytic Materials for Hydrogen Evolution. *Nat. Mater.* **2006**, *5*, 909–913.
- (4) Laursen, L. B.; Kegnaes, S.; Dahla, S.; Chorkendorff, I. Molybdenum Sulfides-Efficient and Viable Materials for Electro and Photoelectrocatalytic Hydrogen Evolution. *Energy Environ. Sci.* **2012**, *5*, 5577–5591.
- (5) Yu, X. Y.; Yu, L.; Lou, X. W. Hollow Nanostructures of Molybdenum Sulfides for Electrochemical Energy Storage and Conversion. *Small Methods* **2017**, *1*, 1600020.
- (6) Jaramillo, T. F.; Jørgensen, K. P.; Bonde, J.; Nielsen, J. H.; Horch, S.; Chorkendorff, I. Identification of Active Edge Sites for Electro-

chemical H₂ Evolution from MoS₂ Nanocatalysts. *Science* **2007**, *317*, 100–102.

(7) Yu, X.; Feng, Y.; Jeon, Y.; Guan, B.; Lou, X.; Paik, U. Formation of Ni–Co–MoS₂ Nanoboxes with Enhanced Electrocatalytic Activity for Hydrogen Evolution. *Adv. Mater.* **2016**, *28*, 9006–9011.

(8) Yu, L.; Xia, B.; Wang, X.; Lou, X. General Formation of M–MoS₂ (M = Co, Ni) Hollow Structures with Enhanced Electrocatalytic Activity for Hydrogen Evolution. *Adv. Mater.* **2016**, *28*, 92–97.

(9) Nørskov, J. K.; Bligaard, T.; Rossmeisl, J.; Christensen, C. H. Towards the Computational Design of Solid Catalysts. *Nat. Chem.* **2009**, *1*, 37–46.

(10) Subbaraman, R.; Tripkovic, D.; Strmcnik, D.; Chang, K. C.; Uchimura, M.; Paulikas, A. P.; Stamenkovic, V.; Markovic, N. M. Enhancing Hydrogen Evolution Activity in Water Splitting by Tailoring Li⁺-Ni(OH)₂-Pt Interfaces. *Science* **2011**, *334*, 1256–1260.

(11) Hou, Y.; Abrams, B. L.; Vesborg, P. C. K.; Björketun, M. E.; Herbst, K.; Bech, L.; Setti, A. M.; Damsgaard, C. D.; Pedersen, T.; Hansen, O.; Rossmeisl, J.; Dahl, S.; Nørskov, J. K.; Chorkendorff, I. Bioinspired Molecular Co-Catalysts Bonded to a Silicon Photocathode for Solar Hydrogen Evolution. *Nat. Mater.* **2011**, *10*, 434–438.

(12) Seger, B.; Laursen, A. B.; Vesborg, P. C. K.; Pedersen, T.; Hansen, O.; Dahl, S.; Chorkendorff, I. Hydrogen Production Using a Molybdenum Sulfide Catalyst on a Titanium-Protected n⁺ p-Silicon Photocathode. *Angew. Chem., Int. Ed.* **2012**, *51*, 9128–9131.

(13) Bollinger, M. V.; Lauritsen, J. V.; Jacobsen, K. W.; Nørskov, J. K.; Helveg, S.; Besenbacher, F. One-Dimensional Metallic Edge States in MoS₂. *Phys. Rev. Lett.* **2001**, *87*, 196803.

(14) Le, G. A.; Artero, V.; Jusselme, B.; Tran, P. D.; Guillet, N.; Métayé, R.; Fihri, A.; Palacin, S.; Fontecave, M. From Hydrogenases to Noble Metal-Free Catalytic Nanomaterials for H₂ Production and Uptake. *Science* **2009**, *326*, 1384–1387.

(15) Karunadasa, H. I.; Chang, C. J.; Long, J. R. A Molecular Molybdenum-Oxo Catalyst for Generating Hydrogen from Water. *Nature* **2010**, *464*, 1329–1333.

(16) Helm, M. L.; Stewart, M. P.; Bullock, R. M.; DuBois, M. Rakowski.; DuBois, L. D. A Synthetic Nickel Electrocatalyst with a Turnover Frequency above 100000 s⁻¹ for H₂ Production. *Science* **2011**, *333*, 863–866.

(17) Karunadasa, H. I.; Montalvo, E.; Sun, Y.; Majda, M.; Long, J. R.; Chang, C. J. A Molecular MoS₂ Edge Site Mimic for Catalytic Hydrogen Generation. *Science* **2012**, *335*, 698–702.

(18) Kibsgaard, J.; Chen, Z.; Reinecke, B. N.; Jaramillo, T. F. Engineering the Surface Structure of MoS₂ to Preferentially Expose Active Edge Sites for Electrocatalysis. *Nat. Mater.* **2012**, *11*, 963–969.

(19) Merki, D.; Hu, X. Recent Developments of Molybdenum and Tungsten Sulfides as Hydrogen Evolution Catalysts. *Energy Environ. Sci.* **2011**, *4*, 3878–3888.

(20) Vrabel, H.; Merki, D.; Hu, X. Hydrogen Evolution Catalyzed by MoS₃ and MoS₂ Particles. *Energy Environ. Sci.* **2012**, *5*, 6136–6144.

(21) Kong, D.; Wang, H.; Cha, J. J.; Pasta, M.; Koski, K. J.; Yao, J.; Cui, Y. Synthesis of MoS₂ and MoSe₂ Films with Vertically Aligned Layers. *Nano Lett.* **2013**, *13*, 1341–1347.

(22) Xie, J.; Zhang, H.; Li, S.; Wang, R.; Sun, X.; Zhou, M.; Zhou, J.; Lou, X. W.; Xie, Y. Defect-Rich MoS₂ Ultrathin Nanosheets with Additional Active Edge Sites for Enhanced Electrocatalytic Hydrogen Evolution. *Adv. Mater.* **2013**, *25*, 5807–5813.

(23) Kibsgaard, J.; Jaramillo, T. F.; Besenbacher, F. Building an Appropriate Active-Site Motif into a Hydrogen-Evolution Catalyst With Thiomolybdate [Mo₃S₁₃]²⁻ Clusters. *Nat. Chem.* **2014**, *6*, 248–253.

(24) Yan, Y.; Xia, B. Y.; Ge, X. M.; Liu, Z. L.; Wang, J. Y.; Wang, X. Ultrathin MoS₂ Nanoplates with Rich Active Sites as Highly Efficient Catalyst for Hydrogen Evolution. *ACS Appl. Mater. Interfaces* **2013**, *5*, 12794–12798.

(25) Li, H.; Tsai, C.; Koh, A. L.; Cai, L.; Contryman, A. W.; Fragapane, A. H.; Zhao, J.; Han, H. S.; Manoharan, H. C.; Pedersen, F. A.; Nørskov, J. K.; Zheng, X. Activating and Optimizing MoS₂ Basal Planes for Hydrogen Evolution Through the Formation of Strained Sulphur Vacancies. *Nat. Mater.* **2016**, *15*, 48–53.

(26) Voiry, D.; Salehi, M.; Silva, R.; Fujita, T.; Chen, M.; Asefa, T.; henoy, V. B.; Eda, S. G.; Chhowalla, M. Conducting MoS₂ Nanosheets as Catalysts for Hydrogen Evolution Reaction. *Nano Lett.* **2013**, *13*, 6222–6227.

(27) Wang, D.; Zhang, X.; Bao, S.; Zhang, Z.; Fei, H.; Wu, Z. Phase engineering of a multiphase 1T/2H MoS₂ catalyst for highly efficient hydrogen evolution. *J. Mater. Chem. A* **2017**, *5*, 2681–2688.

(28) Geng, X.; Sun, W.; Wu, W.; Chen, B.; Hilo, A. A.; Benamara, M.; Zhu, H.; Watanabe, F.; Cui, J.; Chen, T. Pure and Stable Metallic Phase Molybdenum Disulfide Nanosheets for Hydrogen Evolution Reaction. *Nat. Commun.* **2016**, *7*, 10672.

(29) Yin, Y.; Han, J.; Zhang, Y.; Zhang, X.; Xu, P.; Yuan, Q.; Samad, L.; Wang, X.; Wang, Y.; Zhang, Z.; Zhang, P.; Cao, X.; Song, B.; Jin, S. Contributions of Phase, Sulfur Vacancies, and Edges to the Hydrogen Evolution Reaction Catalytic Activity of Porous Molybdenum Disulfide Nanosheets. *J. Am. Chem. Soc.* **2016**, *138*, 7965–7972.

(30) Chou, S. S.; Sai, N.; Lu, P.; Coker, E. N.; Liu, S.; Artyushkova, K.; Luk, T. S.; Kaehr, B.; Brinker, C. J. Understanding Catalysis in a Multiphase Two-Dimensional Transition Metal Dichalcogenide. *Nat. Commun.* **2015**, *6*, 8311.

(31) Li, Y.; Wang, H.; Xie, L.; Liang, Y.; Hong, G.; Dai, H. MoS₂ Nanoparticles Grown on Grapheme: an Advanced Catalyst for the Hydrogen Evolution Reaction. *J. Am. Chem. Soc.* **2011**, *133*, 7296–7299.

(32) Li, D. J.; Maiti, U. N.; Lim, J.; Choi, D. S.; Lee, W. J.; Oh, Y.; Lee, G. Y.; Kim, S. O. Molybdenum Sulfide/N-doped CNT Forest Hybrid Catalysts for High-Performance Hydrogen Evolution Reaction. *Nano Lett.* **2014**, *14*, 1228–1233.

(33) Yang, L.; Zhou, W.; Hou, D.; Zhou, K.; Li, G.; Tang, Z.; Li, L.; Chen, S. Porous metallic MoO₂-supported MoS₂ nanosheets for enhanced electrocatalytic activity in the hydrogen evolution reaction. *Nanoscale* **2015**, *7*, 5203–5208.

(34) Yang, L.; Zhou, W.; Lu, J.; Hou, D.; Ke, Y.; Li, G.; Tang, Z.; Kang, X.; Chen, S. Hierarchical spheres constructed by defect-rich MoS₂/carbon nanosheets for efficient electrocatalytic hydrogen evolution. *Nano Energy* **2016**, *22*, 490–498.

(35) Park, S.; Chung, D.; Ko, D.; Sung, Y.; Piao, Y. Three-dimensional carbon foam/N-doped graphene@MoS₂ hybrid nanostructures as effective electrocatalysts for the hydrogen evolution reaction. *J. Mater. Chem. A* **2016**, *4*, 12720–12725.

(36) Schmidt, H.; Giustiniano, F.; Eda, G. Electronic Transport Properties of Transition Metal Dichalcogenide Field-Effect Devices: Surface and Interface Effects. *Chem. Soc. Rev.* **2015**, *44*, 7715–7736.

(37) Tan, C.; Zhang, H. Two-Dimensional Transition Metal Dichalcogenide Nanosheet-Based Composites. *Chem. Soc. Rev.* **2015**, *44*, 2713–2731.

(38) Eda, G.; Yamaguchi, H.; Voiry, D.; Fujita, T.; Chen, M.; Chhowalla, M. Photoluminescence from Chemically Exfoliated MoS₂. *Nano Lett.* **2011**, *11*, 5111–5116.

(39) Yang, D.; Sandoval, S. J.; Divigalpitiya, W. M. R.; Irwin, J. C.; Frindt, R. F. Structure of Single-Molecular-Layer MoS₂. *Phys. Rev. B: Condens. Matter Mater. Phys.* **1991**, *43*, 12053–12056.

(40) Sandoval, S. J.; Yang, D.; Frindt, R. F.; Irwin, J. C. Raman Study and Lattice Dynamics of Single Molecular Layers of MoS₂. *Phys. Rev. B: Condens. Matter Mater. Phys.* **1991**, *44*, 3955–3962.

(41) Maitra, U.; Gupta, U.; De, M.; Datta, R.; Govindaraj, A.; Rao, C. N. R. Highly Effective Visible-Light-Induced H₂ Generation by Single-Layer 1T-MoS₂ and a Nanocomposite of Few-Layer 2H-MoS₂ with Heavily Nitrogenated Graphene. *Angew. Chem., Int. Ed.* **2013**, *52*, 13057–13061.

(42) Song, L.; Ci, L.; Lv, L.; Zhou, Z.; Yan, X.; Liu, D.; Yuan, H.; Gao, Y.; Wang, J.; Liu, L.; Zhao, X.; Zhang, Z.; Dou, X.; Zhou, W.; Wang, G.; Wang, C.; Xie, S. Direct Synthesis of a Macroscale Single-Walled Carbon Nanotube Non-Woven Material. *Adv. Mater.* **2004**, *16*, 1529–1534.

(43) Liu, Q.; Li, X.; He, Q.; Khalil, A.; Liu, D.; Xiang, T.; Wu, X.; Song, L. Gram-Scale Aqueous Synthesis of Stable Few-Layered 1T-MoS₂: Applications for Visible-Light-Driven Photocatalytic Hydrogen Evolution. *Small* **2015**, *11*, 5556–5564.

(44) Liu, Q.; Shang, Q.; Khalil, A.; Fang, Q.; Chen, S.; He, Q.; Xiang, T.; Liu, D.; Zhang, Q.; Luo, Y.; Song, L. In situ Integration of a Metallic 1T-MoS₂/CdS Heterostructure as a means To Promote Visible-Light-Driven Photocatalytic Hydrogen Evolution. *ChemCatChem* **2016**, *8*, 2614–2619.

(45) Ravel, B.; Newville, M. ATHENA, ARTEMIS, HEPHAESTUS: Data Analysis for X-ray Absorption Spectroscopy using IFEFFIT. *J. Synchrotron Radiat.* **2005**, *12*, 537–541.

(46) Koroteev, V. O.; Bulusheva, L. G.; Asanov, I. P.; Shlyakhova, E. V.; Vyalikh, D. V.; Okotrub, A. V. Charge Transfer in the MoS₂/Carbon Nanotube Composite. *J. Phys. Chem. C* **2011**, *115*, 21199–21204.

(47) Liao, T.; Sun, Z.; Sun, C.; Dou, X. S.; Searles, J. D. Electronic Coupling and Catalytic Effect on H₂ Evolution of MoS₂/Graphene Nanocatalyst. *Sci. Rep.* **2015**, *4*, 6256.

(48) Benck, J. D.; Chen, Z.; Kuritzky, L. Y.; Forman, J. A.; Jaramillo, F. T. Amorphous Molybdenum Sulfide Catalysts for Electrochemical Hydrogen Production: Insights into the Origin of Their Catalytic Activity. *ACS Catal.* **2012**, *2*, 1916–1923.